PROCEEDINGS OF SPIE

SPIEDigitalLibrary.org/conference-proceedings-of-spie

ASTENA: an innovative mission concept for broadband high-energy astrophysics

Enrico Virgilli, Filippo Frontera, Lisa Ferro, Miguel Fernandes Moita, Leo Cavazzini, et al.

Enrico Virgilli, Filippo Frontera, Lisa Ferro, Miguel Fernandes Moita, Leo Cavazzini, Piero Rosati, Cristiano Guidorzi, Mauro Orlandini, Claudio Labanti, Ezio Caroli, Natalia Auricchio, John B. Stephen, Stefano del Sordo, Lorenzo Amati, "ASTENA: an innovative mission concept for broadband high-energy astrophysics," Proc. SPIE 12181, Space Telescopes and Instrumentation 2022: Ultraviolet to Gamma Ray, 121812H (31 August 2022); doi: 10.1117/12.2630080

SPIE.

Event: SPIE Astronomical Telescopes + Instrumentation, 2022, Montréal, Québec, Canada

ASTENA: an innovative mission concept for broadband high-energy astrophysics

Enrico Virgilli[a,b], Filippo Frontera[a,c], Lisa Ferro[c], Miguel Fernandes Moita[c], Leo Cavazzini[c], Piero Rosati[c,a,d], Cristiano Guidorzi[c,a,d], Mauro Orlandini[a], Claudio Labanti[a], Ezio Caroli[a], Natalia Auricchio[a], John B. Stephen[a], Stefano Del Sordo[e], and Lorenzo Amati[a]

[a]INAF/OAS of Bologna, Italy
[b]INFN of Bologna, Italy
[c]Physics and Earth Science Department, University of Ferrara, Italy
[d]INFN of Ferrara, Italy
[e]INAF/IASF of Palermo, Italy

ABSTRACT

Hard-X/soft gamma-rays are probes of the most powerful phenomena in the Universe. Unlike soft x-ray astrophysics, this band has benefited less from the technological advancement due to the difficulty to absorb this radiation and to the lack of focusing instrumentation. For these reasons the quest for innovative soft gamma-ray instrumentation is pressing and their effective recognition and realization are urgent. In this context, and in the framework of the AHEAD project, funded by the European Commission, the ASTENA experiment was proposed as an innovative mission concept to face some of the most debated questions in hard X-/gamma-ray astronomy. This effort will be done through the use of instruments based on groundbreaking technologies, capable of providing unprecedented broad energy passband in a wide field of view, high sensitivity observations and, at the same time, sub-arcminute localization of gamma-ray sources and polarimetric measurement. In this paper we describe the instruments on board ASTENA, the technologies involved, the performances achievable with their exploitation and their level of readiness.

Keywords: hard X-/soft gamma-ray astronomy, Laue lenses, focussing instruments, position sensitive detectors, silicon drift detectors, Cadmium Zinc Telluride.

1. INTRODUCTION

Hard X-/soft gamma-rays represent powerful exploration tools of the inner regions of most energetic and luminous sources in the Universe which involve strong gravitational or electromagnetic fields, extreme temperatures and speed of particles. In recent years, the request for more sophisticated and sensitive instrumentation has become more urgent, pushed both from the modernization of the instrumentation for soft x-rays, which has been relatively more fast with the advent of new detector technologies and multilayer optics, and mostly from the remarkable progress which has been made on the development of gravitational wave detectors which led to the birth of multi-messenger astrophysics.

Among the most important questions in high energy astrophysics, those related to the transient sky and to nuclear astrophysics are the most challenging. Almost all cosmic X-ray sources are highly variable as a function of time on very different time scales from fraction of seconds to years. Spectral and, possibly, imaging on a short time scale are key capabilities in order to understand the physics of these sources. On the other hand, in order to investigate on short time scale the flux variation of a source and/or its short-term spectral evolution, high sensitivity instruments are required and, to this end, large effective areas and/or focusing power are required. On the other side, nuclear astrophysics is observationally underdeveloped with respect to other fields and still based on theoretical models. More sensitive observations are required in order to solve some questions. For instance, the 511 keV emission from the galactic center is due to the annihilation e^+/e^-. Where do the positrons come from? Is this 511 keV radiation originated from discrete and localizable sources?

Corresponding author Enrico Virgilli: E-mail: enrico.virgilli@inaf.it

Space Telescopes and Instrumentation 2022: Ultraviolet to Gamma Ray, edited by Jan-Willem A. den Herder, Shouleh Nikzad, Kazuhiro Nakazawa, Proc. of SPIE Vol. 12181, 121812H · © 2022 SPIE · 0277-786X · doi: 10.1117/12.2630080

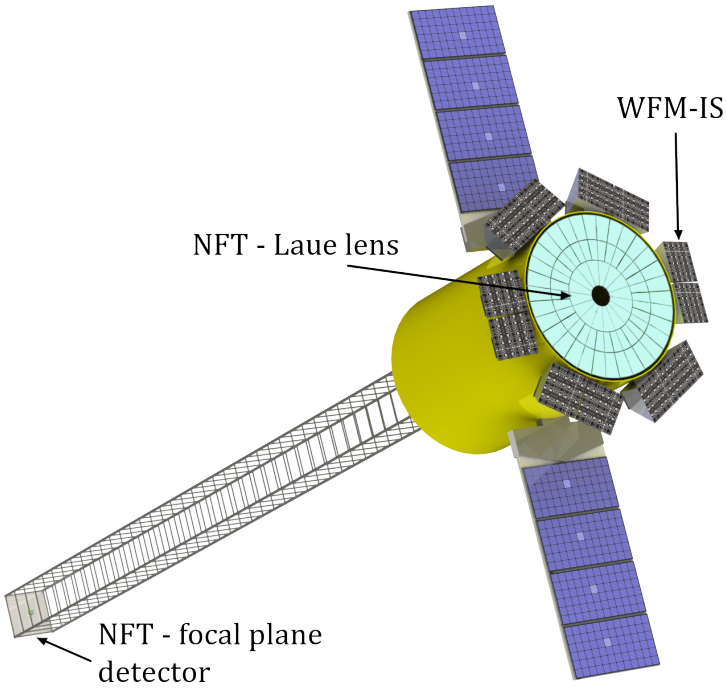

Figure 1. Rendering of the ASTENA mission concept which consists of two coaligned instruments: a Wide Field Monitor-Imaging Spectrometer (WFM-IS) composed by a set of 12 identical cameras, and a Narrow Field Telescope (NFT) based on a 20 m long focal length Laue lens.

We have conceived an experiment that provide large passband with wide field of view observations and high sensitivity observations of finely localized sources. This mission concept has been named ASTENA (Advanced Surveyor of Transient Events and of Nuclear Astrophysics). The ASTENA mission consists of two coaligned instruments with a symmetric layout, as can be seen in Fig 1. The first instrument is a Wide Field Monitor-Imaging Spectrometer (WFM-IS), the second is the Narrow Field Telescope (NFT). The axes of the two instruments are coaligned.

The concept mission ASTENA has been defined in this paper as an *innovative mission* as it is based on three innovative technologies which will be a breakthrough for soft gamma-ray astronomy, allowing performance never achieved so far. These innovative technologies are the following:

- the new concept, and not yet used in a space experiment, of a position sensitive detector based on pixels made from bars of scintillator crystals coupled with Silicon Drift Detectors (SDDs). Such a configuration, that will be described in Sect. 4, allows for the detection of photons in an unprecedented energy passband (2 keV - 20 MeV), with a single compact and highly modular instrument. Such a modularity allows to realize large area detectors with different geometries thus providing very high sensitivity in a wide Field of View (FoV), ideal for a wide sky monitoring;
- an innovative Laue lens that can efficiently focus hard X-/soft gamma-rays within a Point Spread Function (PSF) having a Half Power Diameter (HPD) of the order of 30 arcsec within a FoV of a few arcminutes, ideal for deep observations of localized transients or for high-sensitivity monitoring of known sources. To enable this focusing power we use bent crystals in transmission configuration;
- a focal plane detector for hard X-/soft gamma-rays exploiting the Cadmium Zinc Telluride (CZT) solid state detector technology with fine segmentation in both plane directions by using the drift strip detector concept and providing coordinate identification of the order of a few hundreds microns. The interaction depth (Z-coordinate value) can be inferred from the ratio between the signal collected by anodes and

cathodes electrode strips, arranged perpendicularly to each other on the two different sides of the CZT volume.

The basic form of the SDD was proposed in 1983[1] . In its basic form, it consisted of a volume of fully depleted Silicon, in which an electric field with a strong component parallel to the surface drifts the electrons generated by the absorption of ionising radiation towards a small sized collecting anode. They were proposed for the detection of high energy charged particles and successfully applied for ground experiment (e.g. the ALICE experiment at LHC[2]). SDD have been proposed for different space experiments in the stand-alone version (LOFT[3] , STROBE-X[4]), or coupled with bars of scintillator crystal to extend the working passband at hard-X rays (above 20/30 keV). In the latter case, missions are under evaluation (THESEUS[5] , e-ASTROGAM[6]) accepted (eXTP[7]) or already in the implementation phase (HERMES[8]). For its innovative concept and flexible design, several layouts have been proposed. Moreover, R&D in this field is dynamic as there is still room for innovation to improve performance.

The Laue lens technology has been proposed in the past with different configurations. The Gamma-Ray Imager (GRI[9]) proposal consisted in a Laue lens coupled to a single-reflection multilayer coated concentrator. While the latter was designed to cover the 50-200 keV passband, the Laue lens was proposed for the 200 – 900 keV passband with the goal of reaching 1300 keV. The focal length of the order of 100 m was kept through a formation flying configuration thus with two independent and finely aligned spacecraft. Balloon campaigns (CLAIRE[10]) and laboratory experiments[11,12] have demonstrated the feasibility of this technology and the performances of both narrow and broad passband concentrators.

The gamma-ray detection technology based on CZT/CdTe semiconductor has been already used for the ISGRI instrument[13,14] based on CdTe, the low energy camera of the IBIS imager on board INTEGRAL. However, the passband was limited to the range 15 – 250 keV due to the thickness of the crystals which was 2 mm. In the ASTENA context several layers of CZT detector are stacked together and the so-called Photon Transverse Field (PTF) illumination configuration will be exploited in which the photons enter the detector from the thickness of the crystal and the drift field is perpendicular to the photon entrance direction. With this arrangement a more thick detector is feasible and a high resolution three dimensional (3D) position sensitivity is achievable.

In this article we will describe these three innovative technologies providing details of their working principles, by describing the adopted layout for the specific case of ASTENA and, particularly important, by discussing their present technological readiness which is a crucial parameter in order to propose a mission for the next calls in the national or international context.

2. AN INNOVATIVE DIFFRACTIVE OPTICS

Laue lenses have been proposed in the second half of the last century[15–17] . Concept and science rationale have been also widely described more recently[18] . Since their first proposal, several efforts have been made in both design and experimental validation. The essential elements of a Laue Lens are a large number of high-quality crystals which must be correctly oriented to diffract the radiation in a narrow spectral range from a distant source towards a focal plane detector positioned at a common focus behind the lens (see Fig. 2). Differently from the well known x-ray optics based on grazing incidence and multilayers, which are operative up to 70/80 keV based on Bragg diffraction in reflection configuration, Laue lenses use diffractive crystals in transmission configuration. As a consequence of this, apart from a negligible projection effect, the total crystals surface contribute to the whole concentrator area and their full thickness contribute to the diffraction process differently from the soft X-ray optics in which the Bragg reflection involves less than 1 μm of the crystal thickness[19] . Mosaic flat crystals have been widely used in the past, including for the mentioned experiments on ground and on stratospheric balloons. They have well known limitations. On the one side, the diffraction efficiency is, according to the dynamical theory of diffraction[20] , less than 50% of the incoming flux which limits the throughput of a diffractive optics. On the other side, flat mosaic crystals provide a limited focusing power, as the shadow produced by each flat mosaic crystal has the size of the crystal itself plus a mosaic defocusing[21] which increases as the focal distance increases. Curved crystals represent an alternative to mosaic flat crystals as they overcome the aforementioned limits. Bent perfect crystals does not have the 50% reflectivity limitation and a bent crystal tile behaves as a cylindrical concentrator thus its diffracted footprint is smaller than the cross section of the crystal itself.

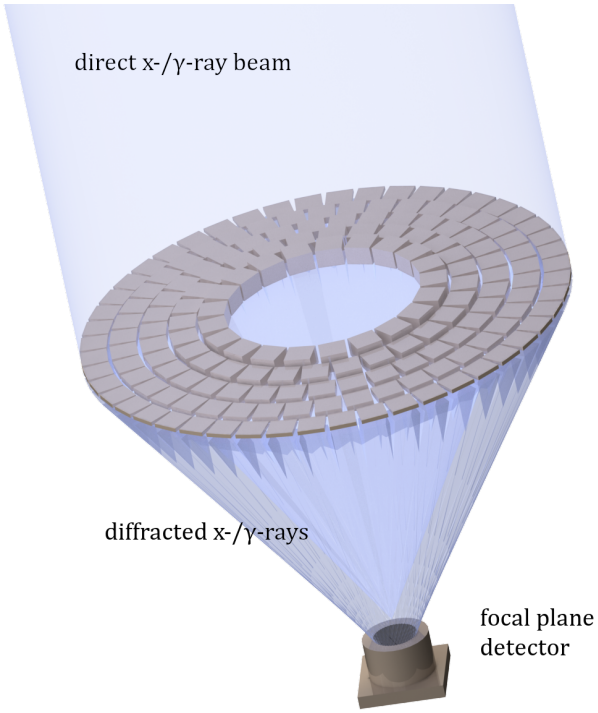

Figure 2. Laue lens concept. A set of crystals are properly oriented according to the Bragg law in order to commonly focus the radiation on a position sensitive detector placed at the focal distance.

2.1 NFT layout and instrument requirements

The NFT optics consists of a Laue lens made with cylindrical bent Silicon Si(111) and Germanium Ge(111) crystals with cross section 30 × 10 mm^2; the longer dimension is the focusing direction. The crystals are oriented and distributed in 43 concentric rings having inner and outer radii of 18 cm and 149 cm, respectively, providing a total geometric area of 7 m^2. The total number of crystals for covering such a collecting area is of the order of 19500. The NFT has a focal length (FL) of 20 m. Taking into account the 5 m long rigid spacecraft body, with the present industrial technologies, a 15 m extendable boom is feasible, therefore the mission can be realised in a single spacecraft configuration. In the present configuration the expandable structure is folded within the rigid cylindrical body that, at launch, holds the focal plane detector and the WFM-IS as well.

Several interesting questions are linked to the sub-MeV domain where the photons are rare. There are only two way to face this limit: the most obvious is to extend the integration time but this would prevent to observe short term source variations. The most compelling way is instead to extend as much as possible the effective area of the instrument. This, together with the capability as a gamma-ray concentrator would lead to unprecedented line and continuum sensitivity which are the main instrument requirements.

The expected sensitivity would lead to the discovery of several new sources of radiation, meaning that a much better angular resolution with respect to non focusing imagers instruments is needed in order to avoid the confusion limit. We have evaluated that an angular resolution of the order of 30" is reasonable and feasible with a Laue lens optics. On the other side, due to the single reflection geometry, strong aberration effects are present for off-axis sources, limiting the FoV. This effect is qualitatively shown in Fig. 3 in which one on-axis source is simulated together with an off-axis source for different off-axis angles. We have estimated that, with the present configuration of the Laue lens, the angular resolution is of the order of 30" within an achievable FoV of ∼4 arcminutes.

2.2 Maturity of the Laue lens technology

Laue lenses offer the possibility of providing sub-arcminute angular resolution. However, this goal is not trivial if flat crystals are used, as the angular resolution depends on both the crystal size and the Laue lens FL. For

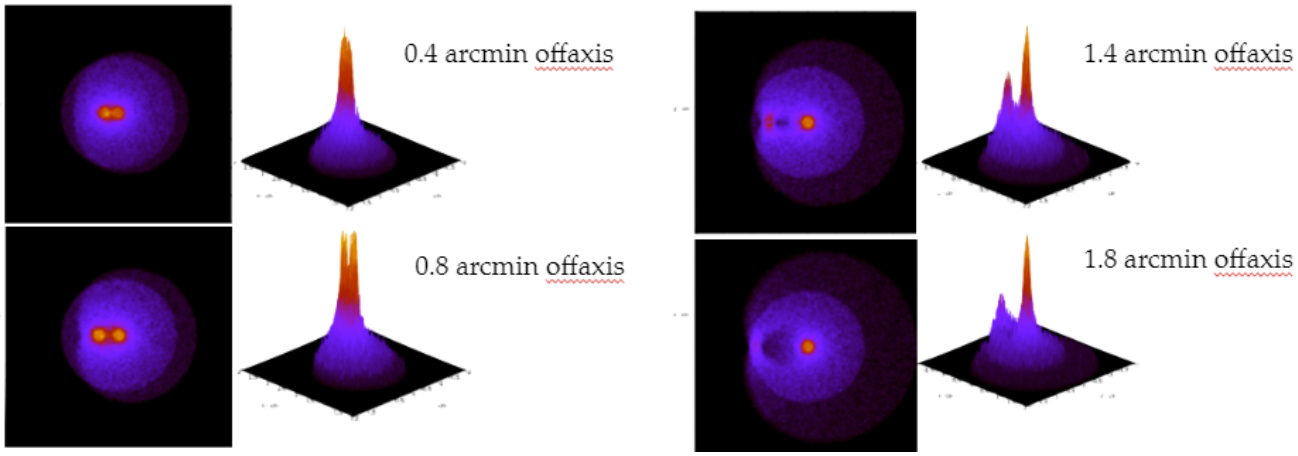

Figure 3. Simulated PSF of one on-axis source together with an off-axis source for different values of the off-axis angle 0.4, 0.8, 1.4 and 1.8 arcminutes. From simulations we evaluated that, with the present NFT configuration, the angular resolution is 30" and the maximum off-axis angle with acceptable Signal to Noise Ratio (SNR) is ∼2", providing a FoV of 4".

instance, flat crystals with cross section 1 × 1 cm^2 and a 20 m FL corresponds to an angular resolving power (α_{rp}) of the order of 1.7 arcminutes which is comparable with that achievable with coded mask techniques (e.g. for INTEGRAL/JEM-X, $\alpha_{rp} \sim 3$ arcmin, for WFC/BeppoSAX, $\alpha_{rp} \sim 5$ arcmin, for CZTI/AstroSAT, $\alpha_{rp} \sim 8$ arcmin). The smaller the crystals size or the longer the FL, the better the achievable α_{rp}. However, a small crystal size implies a large number of tiles, with increasing difficulties in the overall alignment. In the recent past, within the R&D "Laue project" ([22]) bent crystals have been introduced. Bent crystals can overcome this limitation as their diffracted signal is smaller than the crystal cross section itself. Thanks to the bent crystals a PSF comparable to NuSTAR (60" HPD, 18" FWHM) can be achieved or even better with a similar focal length. Several efforts have been made for increasing the TRL of the Laue lenses in the last decade[22,23] . In the activity called TRILL (Technological Readiness Improvement for Laue Lenses)[24] several efforts have been put to maximize the throughput of the Laue lenses. Main goal was to identify the best crystals and the optimal method to manufacture bent crystals. In particular, a repeatable method based on a lapping process on one of the main surfaces have been set up in order to realize accurate bent perfect crystals. Regarding this aspect we have reached a high maturity with a TRL of at least 4. Another important aspect was to find a reproducible and reliable method for the assembly of a large number of crystal tiles in a reasonable short time, high accuracy and with long term stability. Several efforts have been made in order to set at a common focus a large number of crystals over a unique frame. The most obvious solution is to use some kind of adhesive. Unfortunately, every adhesive suffers from a shrinkage process during or after the polymerization phase that unpredictably moves the crystal and worsens the alignment accuracy, making the final PSF wider. Recently, new methods have been proposed in order to set the crystals over a substrate without adhesives. These techniques are under evaluation and test in order to increase the TRL of this process which is, at the moment, 3-4.

3. A CZT FOCAL PLANE DETECTOR WITH 3D CAPABILITY

The development of detectors in the field of the hard X-/ soft gamma-rays has provided in the last decades different concepts that can be used as focal plane devices. Unfortunately, at the moment, none of them provides simultaneous sub-millimetric spatial resolution for fine imaging, high resolution spectroscopy, polarimetric capability and high detection efficiency in the sub-MeV regime that imply a sizeable thickness. All these features are needed for a breakthrough experiment in this energy band. In order to enable hard-X ray imaging and polarimetry, monolithic detectors must be discarded while pixelated or strip detectors represent a suitable solution. However, the drawbacks are a more complex readout circuit and layout structure.

CZT drift strip detectors have a structure similar to the SDD introduced in the eighties[1] . A number of drift strips are interposed between contiguous anode readout strips on one side of the CZT volume. On the other side

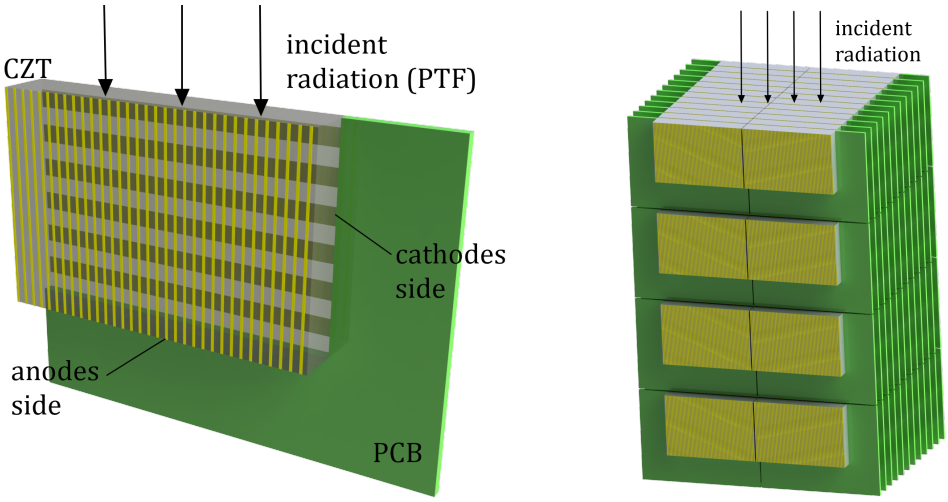

Figure 4. Rendering of the focal plane detector. Left: simplified scheme of a CZT spectrometer sensor with 3D spatial resolution. A single detector consists of a CZT sensor with deposited anode and cathodes on the two opposite sides. Right: the focal plane detector is made of a number of layers of detectors (4 in this example). Within each layer, in order to realize a sufficiently wide area, 2 row of 12 detector each are stacked.

a planar cathode is present or, alternatively, a cathode structure segmented in strips is present with orientation perpendicular to that of the anodes. The anode configuration allows for good spectroscopic performances as it exploits the single-charge carrier collection in which the signal depends only on the electron, avoiding the effects of charge loss due to the hole trapping.

3.1 Geometry and simulated performances

For the ASTENA NFT focal plane detector a multilayer Cadmium Zinc Telluride device is being considered. Simulations have been made to evaluate the minimum detector cross section according to the FoV of the Laue lens, to optimize the detector thickness in order to have a significant detection efficiency at the upper energy threshold and to evaluate the minimum pixel size. In order to consider the whole set of parameters and variables for this task, Monte-Carlo simulations through the MEGAlib software[25] have been done. With MEGAlib, based on Geant4, complex detector geometries can be realized and, through a library of physical interactions, the amount of energy absorbed in the active volume, the number of photons which escape from the sensitive volume, the fraction of photoelectric interaction with respect to the single or multiple Compton interactions can be evaluated.

The detector geometry is presented in Fig. 4 where a single CZT detector and a stack of several detector units are shown. A single detector consists of a CZT crystal with anodes electrode oriented in one direction on one largest side and strips cathodes oriented in the perpendicular direction on the other side. Current technological advancements allow to realize CZT wafers 5 mm thick with 20×30 mm^2 cross section. Passive material like printed circuit board of typical density, required to house ASICs and proximity electronics has been simulated. The PCB is 1 mm thick and 10 mm large along two sides of the CZT crystal is considered in order to leave the other two sides free. This allows to effectively stack several detectors in the so-called PTF (Photons Transverse Field) configuration. From the signal acquired at the anodes, at the cathodes and from the ratio between them is possible to evaluate the three coordinates of interaction with sub-millimetric accuracy.

As the thickness of the detector must be several mm, we investigated how the efficiency and the HPD of the PSF depend on the depth of interaction. Indeed, the absorption of the radiation does not occur at its surface or at a thin layer of the detector which is the case for the detectors used in soft x-ray astronomy. Instead, there is a continuous deposit of energy along the detector thickness. The higher the photon energy to be absorbed, the deeper the photons travel into the detector based on the absorption coefficient of the material. We evaluate the depth of interaction for different monochromatic energies (70, 200, 511, and 700 keV) by simulating the

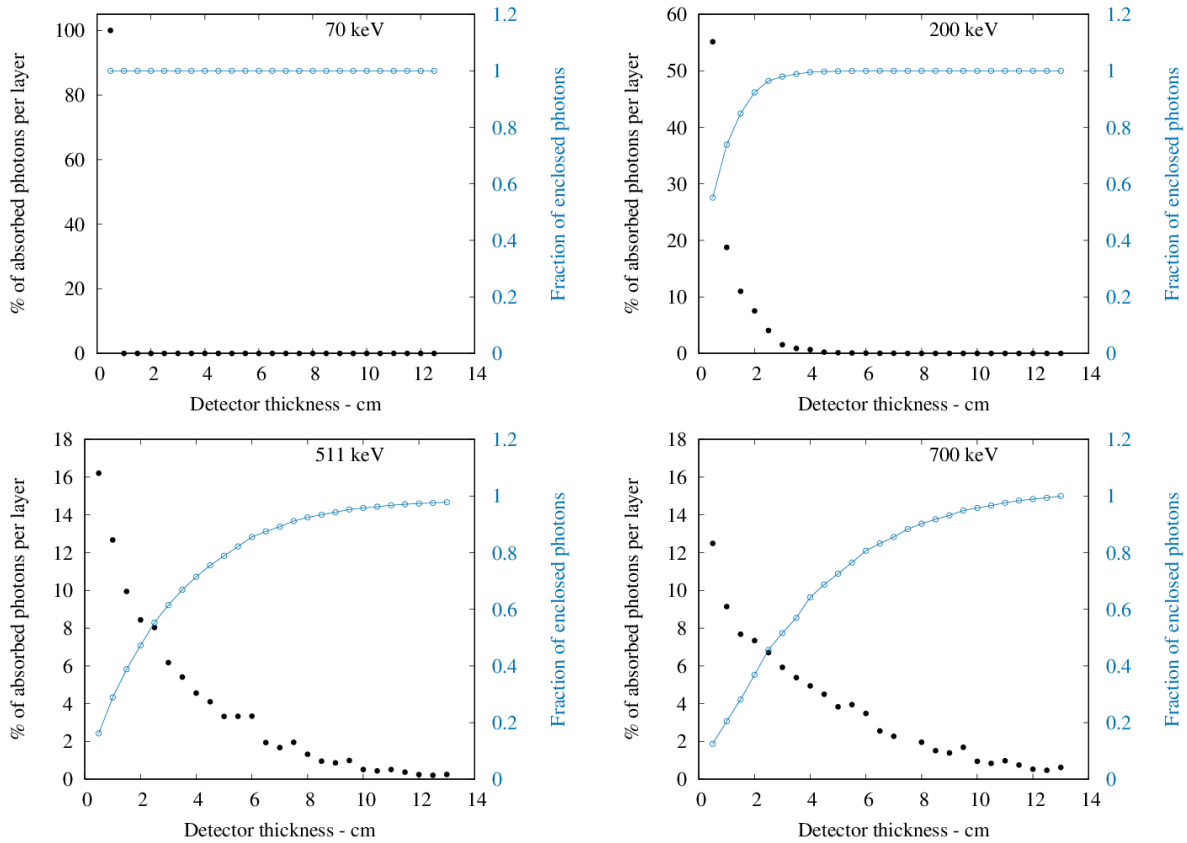

Figure 5. Estimation of the percentage of enclosed photons along the detector thickness with respect to the total enclosed photons (each point corresponds to a layer of 5 mm of active volume) for monochromatic photons with 70, 200, 511, 700 keV. In each graph is also shown the fraction of photons collected by progressively adding the contribution from each layer of the detector.

photons impinging at the detector surface as if they were produced by N crystals radially positioned at the corresponding ring of the Laue lens, therefore N is different for each considered energy, according to the energy-radius relation. These crystals represent N sources of radiation directed towards the detector, instead of being considered diffractive elements of a single infinitely distant source. According to experimental tests and taking into account the size of the crystals, the generated source of radiation have rectangular profile in one direction with 10 mm width and 0.6 mm FWHM in the focusing direction which takes into account for an equivalent spread (*de facto*, the Darwin width) of 5-6 arcsec, as expected for perfect crystals. This simplification allows us to speed-up the Monte-Carlo simulation as only the photons directed towards the detector were simulated without the need to generate several photons from the astrophysical source which does not undergo the diffraction process, thus does not contribute to the overall diffracted image.

An evaluation of the efficiency of interaction as a function of the detector thickness has been done in order to optimize the detector thickness for the instrument energy passband. From Fig. 5, it is evident that low energy photons are stopped in the first millimeters of the detector (0.0008% of the photons interact in the second layer 5 mm thick). Due to the limited cross section of the detector the fraction of photons that escape from the active volume is 2.5% of the total incident photons. As long as the photon energy increases, the interaction depth becomes less negligible. As can be observed, more than 80% of the interactions occur in the first 6 cm of active material. For 700 keV photons the efficiency is of the order of 91%.

For the same energies, we evaluate the profile of the PSF along the detector thickness by determining the fraction of the photons interacting in each detector layer. Through this tomography it is possibile to evaluate how the HPD of the PSF depends on the depth of interaction. In Fig. 6 are reported the fraction of enclosed

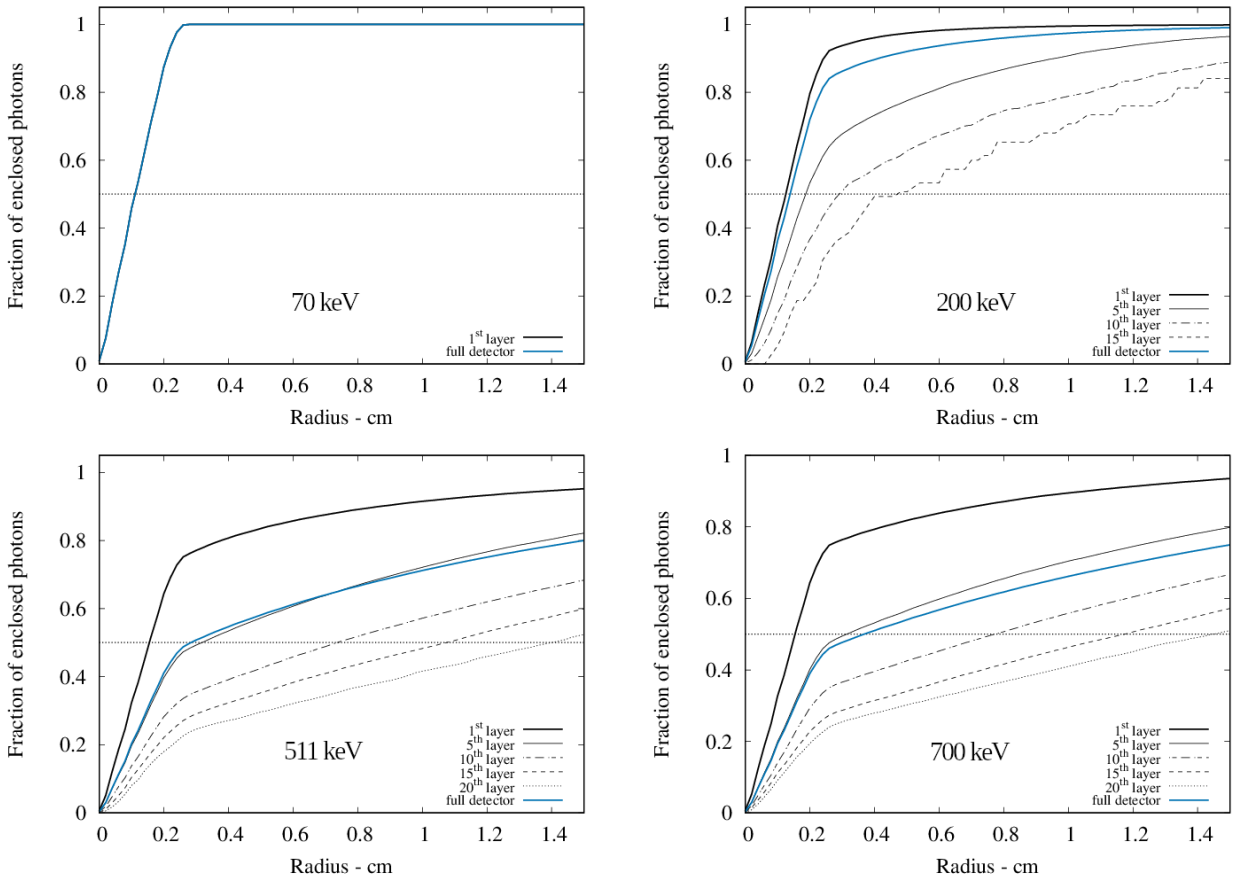

Figure 6. Estimation of the enclosed photons along the detector thickness for monochromatic photons with 70, 200, 511 and 700 keV, respectively.

photons for layers at different depths of the detector (each layer is 5 mm thick of active material) as well as the same fraction by integrating over the whole detector thickness. As can be observed, for 70 keV photons the interaction occurs in the first layer and the HPD is 22.7 arcsec. For 200 keV photons we evaluated an HPD of 25.8" in the first layer. At 500 keV the HPD in the first layer is 31" while for the whole detector we obtain 58". This demonstrates that, in order to the best angular resolution with the NFT, a spatial reconstruction capability along the depth of the detector is required. Further simulations are being performed to optimize the spatial resolution in the depth direction.

3.2 Technological Readiness Level

Pixelated CZT and CdTe have been already used in different space-based experiments. CdTe (16384 units, 4 $\times$ 4 mm^2 large, 2 mm thick) have been adopted in the ISGRI instrument on board INTEGRAL, with a total detector area of $\sim$2600 cm^2. Pixelated CZT crystals with 4 $\times$ 4 mm^2 $\times$ 2 mm thick have been also used in the burst alert telescope (BAT) on board SWIFT[26] with a total area of $\sim$5240 cm^2. Both ISGRI and BAT are direct view devices exploiting the coded mask concept for enabling imaging up to 1 MeV and 150 keV, respectively. The Cadmium–Zinc–Telluride Imager (CZTI) on board AstroSat[27] is sensitive in the energy range 20–150 keV employs an array of CZT detectors, each with 40 mm $\times$ 40 mm area, 5 mm thick. Each detector is further spatially segmented in 256 pixels with a pitch of 2.5 mm. Above $\sim$ 150 keV the detection efficiency rapidly drops due to the reduced crystal thickness.

The main limitation of such configuration of CZT/CdTe detectors is the large pixel size as focal plane detectors need to have a very good spatial pixelization to ensure that the imaging performance satisfies the requirements on

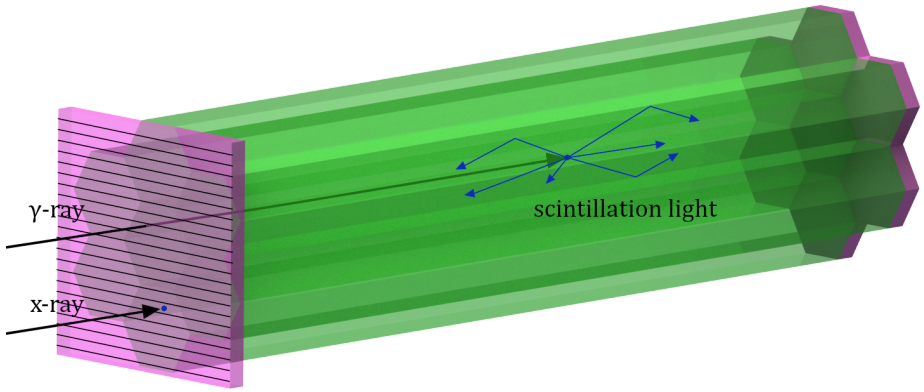

Figure 7. Working principle of the siswich detector system. Two Silicon Drift Detectors (SDDs) are coupled at both sides of a scintillator crystal bars. Low energy photons (¡ 20-30 keV) are directly absorbed in the Silicon while higher energy photons interact in the scintillator bar and the scintillation light is collected by the two SDDs. In this simplification, 7 crystal bars are visible.

angular resolution. Furthermore, the ineffective charge collection, especially for the *holes*, degrades the spectral response. Instead, a very good spectral resolution is required to address astrophysical issues for which a clear line identification is required.

In the last 15 years, several groups have focused their activity on the development of 3D CZT/CdTe with spectroscopic and imaging capabilities with sub-millimetric pixel/voxel size and high detection efficiency. Different approaches have been followed. In the ASTRO-H experiment[28] one layer of CdTe Double-sided Strip Detector (CdTe-DSD) 0.75 mm thick and strip pitch of 250 μm provided an imaging area of 32 $\times$ 32 mm^2. Pixelated detectors provided the capability to operate as a 3D position sensitive spectrometer.[29] Drift strip detectors were developed at DTU Space in the 1990s[30] . CZT drift strip detector (10 mm $\times$ 10 mm $\times$ 2.5 mm) was characterized in the standard illumination configuration and in PTF. The PTF configuration provided a higher efficiency in agreement with calculations. The depth sensing capabilities were tested with an inferred resolution of 90 μm at 122 keV. With the use of CZT drift strip detectors (19.4 $\times$ 19.4 $\times$ 6 mm^3)[31] through the PTF configuration was evaluated an energy resolution of 0.6% at 662 keV. CZT/CdTe (2-d) pixel detector prototypes have been tested to evaluate their polarimetric performances up to 750 keV.[32]

4. THE "SISWICH" CONFIGURATION FOR BROAD ENERGY PASSBAND DETECTOR

The WFM-IS is an array of position sensitive detectors with cross section 43 $\times$ 42 cm, surmounted by two dimensional coded mask at a distance of 70 cm from the detector. The pixelated position sensitive detector is based on the so-called "siswich" (silicon sandwich) configuration[33] which has been proposed for several space and ground experiments (e.g. 3, 7, 34). In Fig. 7 is shown the working principle of the siswich with a sketch showing a limited number of 7 crystals. The basic element of a module is a bar made with a scintillator crystal. The two extremes of the bar are coupled with SDDs for the read-out of the scintillation light, while the other sides of the bar are wrapped with a light reflecting material conveying the scintillation light towards the SDDs. The top-SDD which is facing the sky, representing the X-/gamma-ray entrance window, operates both as X-ray detector for low energy X-ray photons interacting in the Silicon and as a read-out system of the scintillation light produced in the scintillator bar from the interaction with gamma-ray radiation. The bottom-SDD operates as a read-out system for the scintillators and as a discriminator for reducing the instrumental background. The discrimination between energy losses in Si and CsI is based on the different shape of charge pulses.

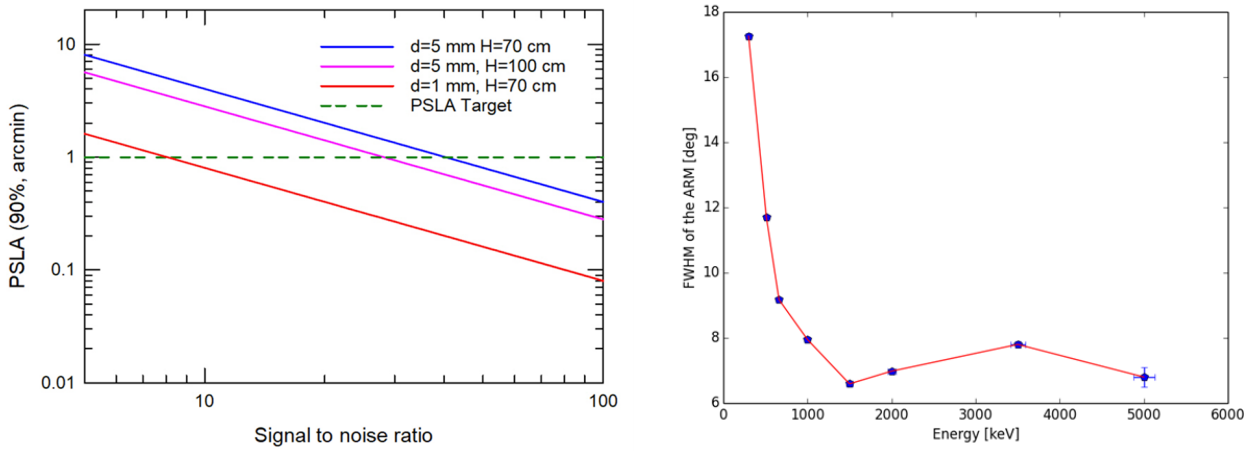

Figure 8. Left: estimated Point Source Location Accuracy (PSLA) at low energies for different values of the coded mask pixel size (d) and mask-detector size (H). Right: estimated PSLA through the Compton kinematics by exploiting all Compton events occurring in each of the 12 WFM-IS cameras.

4.1 Geometry proposed for ASTENA and performances

The WFM-IS consists of 12 identical units distributed around the NFT gamma-ray concentrator. Each unit is made with 4 × 8 modules and each module is composed by 205 pixels. Each pixel is composed by a scintillator crystal bar with regular hexagonal cross section (2.89 mm side resulting in an apothem of 2.5 mm) and 50 mm long, coupled at both sides with SDDs. On the top side of the bar (the one facing the sky) a linear multi-anode SDD is used. This provides a localization capability of the order of 1 arcmin in one direction. By orienting two cameras at 90 degrees it is possible to achieve the 2D localization. On the bottom side the signal by each bar is readout by hexagonal single anode SDDs whose role is to enable gamma-ray polarimetry through Compton reconstruction. The hexagonal shape reduces azimuthal systematic effects as square pixels introduce a strong asymmetry every 90 degrees while hexagon ones provide a more uniform response which is, however, affected by a periodicity of 60 degrees.

Simulations have been performed in order to evaluate the localization accuracy for point sources in the energy range below 30 keV as a function of the significance of the observed source, by considering different ratios between coded mask pixel size and distance between mask and detector (Fig. 8 left). The localization accuracy has been also estimated through Compton kinematic reconstruction in order to enable crude localization at energies in which the WFM-IS is a full sky detector and the mask is fully transparent (Fig. 8 right). As can be observed a localization accuracy of the order of 8-10 degrees can be achieved above 1 MeV. Further techniques for improving the localization accuracy are being implemented, including the exploitation of the different count rate measured by each camera, due to their different orientation with respect to the payload axis.

4.2 Technological maturity

The WFM-IS is based on the SDD and ASIC technologies that have been largely developed in the last 15 years within several R&D projects (XDXL - X-ray Detectors eXtra-Large, REDSoX - REsearch Drift for SOft X-rays and REDSoX-2) by the collaborations between INAF, INFN, FBK (Fondazione Bruno Kessler) and the Universities of Milano-Politecnico and Pavia. The design and manufacture of the SDD (INFN and FBK) has been constantly improved allowing to develop and test SDDs, single or arrays, in different sizes and topologies. Different families of ASIC have been designed (Universities of Milano-Politecnico and University of Pavia) and tested. The LYRA ASIC consists of a single pre-amplifier on a small chip and the remaining circuits in a separated chip while in the last version the ORION ASIC contains also an internal Analog-to-Digital Converter (ADC) for each channel. These layouts have been adopted for the design of detectors for space missions and mission-concepts like HERMES, LOFT, eXTP, THESEUS, e-ASTROGAM, ALBATROS and now for the WFM-IS on board ASTENA as well.

These technologies have been further boosted by the Phase-A study of the THESEUS mission (and in particular for the XGIS instrument), recently re-submitted for ESA/M7. During the Phase-A a module of XGIS has been realized by OHB-Italy in collaboration with ASI and INAF-OAS, supported by ESA. The module has been tested before and after vacuum and thermal cycles. At the moment, it has been recognized that the ASIC technology has reached the TRL of at least 4 while the SDD + CsI scintillator crystals have reached a TRL of 5. Other scintillator materials are being investigated, including the Cerium-doped Gadolinium Aluminium Gallium Garnet GAGG(Ce), already adopted for the HERMES nanosat constellation.

The linear SDD proposed for the top read-out of the WFM-IS has been already used for ground experiments and tested for space application therefore a high TRL is already available. Concerning the bottom part of the readout, hexagonal SDDs have been already realized by FBK therefore further R&D on this technology does not represent a critical activity. On the other hand, the mechanical structure for the packaging of a module in which SDDs and hexagonal scintillator bars are coupled has not been defined yet, therefore further activities are required on this side.

5. CONCLUSIONS

In this paper we have presented the ASTENA mission concept with the special focus of describing the three proposed technologies which are at the foundation of the two on-board instruments.

The first instrument consists of a wide field monitor with a broad energy passband and high sensitivity, consequence of an effective area which is more than 10 times that of the XGIS instrument proposed for the THESEUS mission. SImilarly to XGIS, the WFM-IS allows to perform imaging up to 150 keV by exploiting the classical image reconstruction through coded aperture. Above 150 keV we plan to enable crude localization capability outside the imaging FoV by exploiting Compton kinematic reconstruction as well as the differential flux measured from each camera, as they are differently oriented with respect to the payload axis. Both methods have been preliminary analysed through Monte-Carlo simulations and semi-analytical models with promising results. The WFM-IS is based on the coupling between SDD and scintillator crystals. Such devices have already a high TRL due to a long R&D activity performed in the last 15 years on both SDD and ASIC.

The second instrument is a narrow field telescope based on an innovative Laue lens made with perfect bent Si and Ge crystals with optimized thickness. The use of the higher diffraction orders sensibly increases the overall effective area. Laue lenses have been extensively studied in the last 10 years. Their technological readiness is progressively increasing also thanks to the advent of new materials. The Laue lens needs a CZT detector finely segmented in the three directions. In particular, thanks to the reconstruction in the z direction it will be possible to minimize the HPD of the PSF, thus the NFT sensitivity and imaging capability. The depth resolution will also enable gamma-ray polarimetry. R&D activity in this field is still ongoing in order to optimize the performance.

To conclude we remark that, thanks to the combination and synergy between a wide FoV, high sensitivity, large passband, fast timing instrument with a hard X-ray concentrator capable of localizing sources with sub-arcmin accuracy (never achieved before in this energy passband), ASTENA will be a powerful tool to enhance our knowledge in the field of gamma-ray transient sky and in nuclear astrophysics.

ACKNOWLEDGMENTS

This work is partly supported by the AHEAD-2020 Project grant agreement 871158 of the European Union's Horizon 2020 Programme and by the ASI-INAF agreement no. 2017-14-H.O "Studies for future scientific missions".

REFERENCES

[1] Gatti, E. and Rehak, P., "Semiconductor drift chamber — an application of a novel charge transport scheme," *Nuclear Instruments and Methods in Physics Research* **225**(3), 608–614 (1984).

[2] Rashevsky, A., Bonvicini, V., Burger, P., Piano, S., Piemonte, C., and Vacchi, A., "Large area silicon drift detector for the alice experiment," *Nuclear Instruments and Methods in Physics Research Section A: Accelerators, Spectrometers, Detectors and Associated Equipment* **485**(1), 54–60 (2002). Proceedings of the 5th International Conference on Large Scale Ap plications and Radiation Hardness of Semiconductor Detectors.

[3] Feroci, M., Stella, L., van der Klis, M., Courvoisier, T. J. L., Hernanz, M., Hudec, R., Santangelo, A., Walton, D., Zdziarski, A., Barret, D., Belloni, T., Braga, J., Brandt, S., Budtz-Jørgensen, C., Campana, S., den Herder, J. W., Huovelin, J., Israel, G. L., Pohl, M., Ray, P., Vacchi, A., Zane, S., Argan, A., Attinà, P., Bertuccio, G., Bozzo, E., Campana, R., Chakrabarty, D., Costa, E., De Rosa, A., Del Monte, E., Di Cosimo, S., Donnarumma, I., Evangelista, Y., Haas, D., Jonker, P., Korpela, S., Labanti, C., Malcovati, P., Mignani, R., Muleri, F., Rapisarda, M., Rashevsky, A., Rea, N., Rubini, A., Tenzer, C., Wilson-Hodge, C., Winter, B., Wood, K., Zampa, G., Zampa, N., Abramowicz, M. A., Alpar, M. A., Altamirano, D., Alvarez, J. M., Amati, L., Amoros, C., Antonelli, L. A., Artigue, R., Azzarello, P., Bachetti, M., Baldazzi, G., Barbera, M., Barbieri, C., Basa, S., Baykal, A., Belmont, R., Boirin, L., Bonvicini, V., Burderi, L., Bursa, M., Cabanac, C., Cackett, E., Caliandro, G. A., Casella, P., Chaty, S., Chenevez, J., Coe, M. J., Collura, A., Corongiu, A., Covino, S., Cusumano, G., D'Amico, F., Dall'Osso, S., De Martino, D., De Paris, G., Di Persio, G., Di Salvo, T., Done, C., Dovčiak, M., Drago, A., Ertan, U., Fabiani, S., Falanga, M., Fender, R., Ferrando, P., Della Monica Ferreira, D., Fraser, G., Frontera, F., Fuschino, F., Galvez, J. L., Gandhi, P., Giommi, P., Godet, O., Göğüş, E., Goldwurm, A., Götz, D., Grassi, M., Guttridge, P., Hakala, P., Henri, G., Hermsen, W., Horak, J., Hornstrup, A., in't Zand, J. J. M., Isern, J., Kalemci, E., Kanbach, G., Karas, V., Kataria, D., Kennedy, T., Klochkov, D., Kluźniak, W., Kokkotas, K., Kreykenbohm, I., Krolik, J., Kuiper, L., Kuvvetli, I., Kylafis, N., Lattimer, J. M., Lazzarotto, F., Leahy, D., Lebrun, F., Lin, D., Lund, N., Maccarone, T., Malzac, J., Marisaldi, M., Martindale, A., Mastropietro, M., McClintock, J., McHardy, I., Mendez, M., Mereghetti, S., Miller, M. C., Mineo, T., Morelli, E., Morsink, S., Motch, C., Motta, S., Muñoz-Darias, T., Naletto, G., Neustroev, V., Nevalainen, J., Olive, J. F., Orio, M., Orlandini, M., Orleanski, P., Ozel, F., Pacciani, L., Paltani, S., Papadakis, I., Papitto, A., Patruno, A., Pellizzoni, A., Petráček, V., Petri, J., Petrucci, P. O., Phlips, B., Picolli, L., Possenti, A., Psaltis, D., Rambaud, D., Reig, P., Remillard, R., Rodriguez, J., Romano, P., Romanova, M., Schanz, T., Schmid, C., Segreto, A., Shearer, A., Smith, A., Smith, P. J., Soffitta, P., Stergioulas, N., Stolarski, M., Stuchlik, Z., Tiengo, A., Torres, D., Török, G., Turolla, R., Uttley, P., Vaughan, S., Vercellone, S., Waters, R., Watts, A., Wawrzaszek, R., Webb, N., Wilms, J., Zampieri, L., Zezas, A., and Ziolkowski, J., "The Large Observatory for X-ray Timing (LOFT)," *Experimental Astronomy* **34**, 415–444 (Oct. 2012).

[4] Ray, P. S., Arzoumanian, Z., Ballantyne, D., Bozzo, E., Brandt, S., Brenneman, L., Chakrabarty, D., Christophersen, M., DeRosa, A., Feroci, M., Gendreau, K., Goldstein, A., Hartmann, D., Hernanz, M., Jenke, P., Kara, E., Maccarone, T., McDonald, M., Nowak, M., Phlips, B., Remillard, R., Stevens, A., Tomsick, J., Watts, A., Wilson-Hodge, C., Wood, K., Zane, S., Ajello, M., Alston, W., Altamirano, D., Antoniou, V., Arur, K., Ashton, D., Auchettl, K., Ayres, T., Bachetti, M., Balokovic, M., Baring, M., Baykal, A., Begelman, M., Bhat, N., Bogdanov, S., Briggs, M., Bulbul, E., Bult, P., Burns, E., Cackett, E., Campana, R., Caspi, A., Cavecchi, Y., Chenevez, J., Cherry, M., Corbet, R., Corcoran, M., Corsi, A., Degenaar, N., Drake, J., Eikenberry, S., Enoto, T., Fragile, C., Fuerst, F., Gandhi, P., Garcia, J., Goldstein, A., Gonzalez, A., Grefenstette, B., Grinberg, V., Grossan, B., Guillot, S., Guver, T., Haggard, D., Heinke, C., Heinz, S., Hemphill, P., Homan, J., Hui, M., Huppenkothen, D., Ingram, A., Irwin, J., Jaisawal, G., Jaodand, A., Kalemci, E., Kaplan, D., Keek, L., Kennea, J., Kerr, M., van der Klis, M., Kocevski, D., Koss, M., Kowalski, A., Lai, D., Lamb, F., Laycock, S., Lazio, J., Lazzati, D., Longcope, D., Loewenstein, M., Maitra, D., Majid, W., Maksym, W. P., Malacaria, C., Margutti, R., Martindale, A., McHardy, I., Meyer, M., Middleton, M., Miller, J., Miller, C., Motta, S., Neilsen, J., Nelson, T., Noble, S., O'Brien, P., Osborne, J., Osten, R., Ozel, F., Palliyaguru, N., Pasham, D., Patruno, A., Pelassa, V., Petropoulou, M., Pilia, M., Pohl, M., Pooley, D., Prescod-Weinstein, C., Psaltis, D., Raaijmakers, G., Reynolds, C., Riley, T. E., Salvesen, G., Santangelo, A., Scaringi, S., Schanne, S., Schnittman, J., Smith, D., Smith, K. L., Snios, B., Steiner, A., Steiner, J., Stella, L., Strohmayer, T., Sun, M., Tauris, T., Taylor, C., Tohuvavohu, A., Vacchi, A., Vasilopoulos, G., Veledina, A., Walsh, J., Weinberg, N., Wilkins, D., Willingale, R., Wilms,

J., Winter, L., Wolff, M., Zand, J. i. t., Zezas, A., Zhang, B., and Zoghbi, A., "Strobe-x: X-ray timing and spectroscopy on dynamical timescales from microseconds to years," (2019).

[5] Amati, L., O'Brien, P., Götz, D., Bozzo, E., Tenzer, C., Frontera, F., Ghirlanda, G., Labanti, C., Osborne, J. P., Stratta, G., Tanvir, N., Willingale, R., Attina, P., Campana, R., Castro-Tirado, A. J., Contini, C., Fuschino, F., Gomboc, A., Hudec, R., Orleanski, P., Renotte, E., Rodic, T., Bagoly, Z., Blain, A., Callanan, P., Covino, S., Ferrara, A., Le Floch, E., Marisaldi, M., Mereghetti, S., Rosati, P., Vacchi, A., D'Avanzo, P., Giommi, P., Piranomonte, S., Piro, L., Reglero, V., Rossi, A., Santangelo, A., Salvaterra, R., Tagliaferri, G., Vergani, S., Vinciguerra, S., Briggs, M., Campolongo, E., Ciolfi, R., Connaughton, V., Cordier, B., Morelli, B., Orlandini, M., Adami, C., Argan, A., Atteia, J. L., Auricchio, N., Balazs, L., Baldazzi, G., Basa, S., Basak, R., Bellutti, P., Bernardini, M. G., Bertuccio, G., Braga, J., Branchesi, M., Brandt, S., Brocato, E., Budtz-Jorgensen, C., Bulgarelli, A., Burderi, L., Camp, J., Capozziello, S., Caruana, J., Casella, P., Cenko, B., Chardonnet, P., Ciardi, B., Colafrancesco, S., Dainotti, M. G., D'Elia, V., De Martino, D., De Pasquale, M., Del Monte, E., Della Valle, M., Drago, A., Evangelista, Y., Feroci, M., Finelli, F., Fiorini, M., Fynbo, J., Gal-Yam, A., Gendre, B., Ghisellini, G., Grado, A., Guidorzi, C., Hafizi, M., Hanlon, L., Hjorth, J., Izzo, L., Kiss, L., Kumar, P., Kuvvetli, I., Lavagna, M., Li, T., Longo, F., Lyutikov, M., Maio, U., Maiorano, E., Malcovati, P., Malesani, D., Margutti, R., Martin-Carrillo, A., Masetti, N., McBreen, S., Mignani, R., Morgante, G., Mundell, C., Nargaard-Nielsen, H. U., Nicastro, L., Palazzi, E., Paltani, S., Panessa, F., Pareschi, G., Pe'er, A., Penacchioni, A. V., Pian, E., Piedipalumbo, E., Piran, T., Rauw, G., Razzano, M., Read, A., Rezzolla, L., Romano, P., Ruffini, R., Savaglio, S., Sguera, V., Schady, P., Skidmore, W., Song, L., Stanway, E., Starling, R., Topinka, M., Troja, E., van Putten, M., Vanzella, E., Vercellone, S., Wilson-Hodge, C., Yonetoku, D., Zampa, G., Zampa, N., Zhang, B., Zhang, B. B., Zhang, S., Zhang, S. N., Antonelli, A., Bianco, F., Boci, S., Boer, M., Botticella, M. T., Boulade, O., Butler, C., Campana, S., Capitanio, F., Celotti, A., Chen, Y., Colpi, M., Comastri, A., Cuby, J. G., Dadina, M., De Luca, A., Dong, Y. W., Ettori, S., Gandhi, P., Geza, E., Greiner, J., Guiriec, S., Harms, J., Hernanz, M., Hornstrup, A., Hutchinson, I., Israel, G., Jonker, P., Kaneko, Y., Kawai, N., Wiersema, K., Korpela, S., Lebrun, V., Lu, F., MacFadyen, A., Malaguti, G., Maraschi, L., Melandri, A., Modjaz, M., Morris, D., Omodei, N., Paizis, A., Páta, P., Petrosian, V., Rachevski, A., Rhoads, J., Ryde, F., Sabau-Graziati, L., Shigehiro, N., Sims, M., Soomin, J., Szécsi, D., Urata, Y., Uslenghi, M., Valenziano, L., Vianello, G., Vojtech, S., Watson, D., and Zicha, J., "The THESEUS space mission concept: science case, design and expected performances," *Advances in Space Research* **62**, 191–244 (July 2018).

[6] De Angelis, A., Tatischeff, V., Argan, A., Brandt, S., Bulgarelli, A., Bykov, A., Costantini, E., da Silva, R. C., Grenier, I. A., Hanlon, L., Hartmann, D., Hernanz, M., Kanbach, G., Kuvvetli, I., Laurent, P., Mazziotta, M. N., McEnery, J., Morselli, A., Nakazawa, K., Oberlack, U., Pearce, M., Rico, J., Tavani, M., von Ballmoos, P., Walter, R., Wu, X., Zane, S., Zdziarski, A., and Zoglauer, A., "Gamma-ray astrophysics in the mev range: the astrogam concept and beyond," (2021).

[7] Zhang, S., Santangelo, A., Feroci, M., Xu, Y., Lu, F., Chen, Y., Feng, H., Zhang, S., Brandt, S., Hernanz, M., Baldini, L., Bozzo, E., Campana, R., De Rosa, A., Dong, Y., Evangelista, Y., Karas, V., Meidinger, N., Meuris, A., Nandra, K., Pan, T., Pareschi, G., Orleanski, P., Huang, Q., Schanne, S., Sironi, G., Spiga, D., Svoboda, J., Tagliaferri, G., Tenzer, C., Vacchi, A., Zane, S., Walton, D., Wang, Z., Winter, B., Wu, X., in't Zand, J. J. M., Ahangarianabhari, M., Ambrosi, G., Ambrosino, F., Barbera, M., Basso, S., Bayer, J., Bellazzini, R., Bellutti, P., Bertucci, B., Bertuccio, G., Borghi, G., Cao, X., Cadoux, F., Campana, R., Ceraudo, F., Chen, T., Chen, Y., Chevenez, J., Civitani, M., Cui, W., Cui, W., Dauser, T., Del Monte, E., Di Cosimo, S., Diebold, S., Doroshenko, V., Dovciak, M., Du, Y., Ducci, L., Fan, Q., Favre, Y., Fuschino, F., Gálvez, J. L., Gao, M., Ge, M., Gevin, O., Grassi, M., Gu, Q., Gu, Y., Han, D., Hong, B., Hu, W., Ji, L., Jia, S., Jiang, W., Kennedy, T., Kreykenbohm, I., Kuvvetli, I., Labanti, C., Latronico, L., Li, G., Li, M., Li, X., Li, W., Li, Z., Limousin, O., Liu, H., Liu, X., Lu, B., Luo, T., Macera, D., Malcovati, P., Martindale, A., Michalska, M., Meng, B., Minuti, M., Morbidini, A., Muleri, F., Paltani, S., Perinati, E., Picciotto, A., Piemonte, C., Qu, J., Rachevski, A., Rashevskaya, I., Rodriguez, J., Schanz, T., Shen, Z., Sheng, L., Song, J., Song, L., Sgro, C., Sun, L., Tan, Y., Uttley, P., Wang, B., Wang, D., Wang, G., Wang, J., Wang, L., Wang, Y., Watts, A. L., Wen, X., Wilms, J., Xiong, S., Yang, J., Yang, S., Yang, Y., Yu, N., Zhang, W., Zampa, G., Zampa, N., Zdziarski, A. A., Zhang, A., Zhang, C., Zhang, F., Zhang, L., Zhang, T., Zhang, Y., Zhang, X., Zhang, Z., Zhao, B., Zheng, S., Zhou, Y., Zorzi, N., and Zwart, J. F., "The enhanced X-ray

Timing and Polarimetry mission—eXTP," *Science China Physics, Mechanics, and Astronomy* **62**, 29502 (Feb. 2019).

[8] Fiore, F., Burderi, L., Salvo, T. D., Feroci, M., Labanti, C., Lavagna, M. R., and Pirrotta, S., "HERMES: a swarm of nano-satellites for high energy astrophysics and fundamental physics," in [*Space Telescopes and Instrumentation 2018: Ultraviolet to Gamma Ray*], den Herder, J.-W. A., Nikzad, S., and Nakazawa, K., eds., **10699**, International Society for Optics and Photonics, SPIE (2018).

[9] Knodlseder, J., "GRI: The gamma-ray imager mission," *Advances in Space Research* **40**(8), 1263–1267 (2007).

[10] von Ballmoos, P., Halloin, H., Paul, J., Abrosimov, N., Andersen, K., Astier, P., Basa, S., Barret, D., Bastie, P., Bazzano, A., Bignami, A., Blanchard, A., Cordier, B., Courvoisier, T., Courtois, P., Ealet, A., Hamelin, B., Harris, M., Hernanz, M., Isern, J., Jean, P., Knödlseder, J., Laurent, P., Lebrun, F., Leyre, X., Limousin, O., Marcowith, A., Martinot, V., Mazure, A., Natalucci, L., Olive, J.-F., Pain, R., Paltani, S., Prantzos, N., Riemann, H., Sadat, R., Sainct, H., Skinner, G., Smither, R. K., Ubertini, P., Vedrenne, F., and Weidenspointner, G., "The MAX Mission: Focusing on High-Sensitivity Gamma-Ray Spectroscopy," in [*5th INTEGRAL Workshop on the INTEGRAL Universe*], Schoenfelder, V., Lichti, G., and Winkler, C., eds., *ESA Special Publication* **552**, 747 (Oct. 2004).

[11] Frontera, F., Loffredo, G., Pisa, A., Milani, L., Nobili, F., Auricchio, N., Carassiti, V., Evangelisti, F., Landi, L., Squerzanti, S., Andersen, K. H., Courtois, P., Amati, L., Caroli, E., Landini, G., Silvestri, S., Stephen, J. B., Poulsen, J. M., Negri, B., and Pareschi, G., "Development status of a Laue lens project for gamma-ray astronomy," in [*Proceedings of the SPIE*], **6688** (Sept. 2007).

[12] Virgilli, E., Frontera, F., Valsan, V., Liccardo, V., Carassiti, V., Evangelisti, F., and Squerzanti, S., "Laue lenses for hard x-/soft γ-rays: new prototype results," in [*Proceedings of the SPIE*], **8147, id. 81471B 9 pp.**, 20–29 (2011).

[13] Limousin, O., Duda, J.-M., Lebrun, F., and Leray, J.-P., "The basic component of the isgri cdte gamma-ray camera for space telescope ibis on board the integral satellite," *Nuclear Instruments and Methods in Physics Research Section A: Accelerators, Spectrometers, Detectors and Associated Equipment* **428**(1), 216–222 (1999).

[14] Lebrun, F., Leray, J. P., Lavocat, P., Crétolle, J., Arquès, M., Blondel, C., Bonnin, C., Bouère, A., Cara, C., Chaleil, T., Daly, F., Desages, F., Dzitko, H., Horeau, B., Laurent, P., Limousin, O., Mathy, F., Mauguen, V., Meignier, F., Molinié, F., Poindron, E., Rouger, M., Sauvageon, A., and Tourrette, T., "ISGRI: The INTEGRAL Soft Gamma-Ray Imager," *A&A* **411**, L141–L148 (Nov. 2003).

[15] Lindquist, T. R. and Webber, W. R., "A focusing X-ray telescope for use in the study of extraterrestrial X-ray sources in the energy range 20-140 keV," *Canadian Journal of Physics Supplement* **46**, 1103 (Jan. 1968).

[16] Smither, R. K., "New method for focusing x rays and gamma rays," *Review of Scientific Instruments* **53**, 131–141 (Feb. 1982).

[17] Lund, N., "A Study of Focusing Telescopes for Soft Gamma-Rays," *Experimental Astronomy* **2**, 259–273 (Sept. 1992).

[18] Frontera, F. and Von Ballmoos, P., "Laue gamma-ray lenses for space astrophysics: status and prospects," *Special Issue - X-Ray Focusing: Techniques and Applications* (2010).

[19] Christensen, F. E., Jakobsen, A. C., Brejnholt, N. F., Madsen, K. K., Hornstrup, A., Westergaard, N. J., Momberg, J., Koglin, J., Fabricant, A. M., Stern, M., Craig, W. W., Pivovaroff, M. J., and Windt, D., "Coatings for the NuSTAR mission," in [*Optics for EUV, X-Ray, and Gamma-Ray Astronomy V*], O'Dell, S. L. and Pareschi, G., eds., **8147**, 298 – 316, International Society for Optics and Photonics, SPIE (2011).

[20] Authier, A., [*Dynamical Theory of X-Ray Diffraction*], vol. 11, 534–551 (01 2001).

[21] Lund, N., "An "ESA-Affordable" Laue-lens," *Experimental Astronomy* **20**, 211–217 (Dec. 2005).

[22] Frontera, F., Virgilli, E., Liccardo, V., Valsan, V., Carassiti, V., Chiozzi, S., Evangelisti, F., Squerzanti, S., Statera, M., Guidi, V., Ferrari, C., Zappettini, R. A., Caroli, E., Auricchio, N., Silvestri, S., Camattari, R., Cassese, F., Recanatesi, L., Pecora, M., Mottini, S., and Negri, B., "Development status of the LAUE project," in [*SPIE Proceedings*], Takahashi, T., Murray, S. S., and den Herder, J.-W. A., eds., SPIE (sep 2012).

[23] Barrière, N. M., Tomsick, J. A., Boggs, S. E., Lowell, A., Wade, C., Baugh, M., von Ballmoos, P., Abrosimov, N. V., and Hanlon, L., "Developing a method for soft gamma-ray laue lens assembly and calibration," *Nuclear Instruments and Methods in Physics Research Section A: Accelerators, Spectrometers, Detectors and Associated Equipment* **741**, 47–56 (2014).

[24] Ferro, L., Virgilli, E., Moita, M. F., Frontera, F., Rosati, P., Guidorzi, C., et al., "The TRILL project and its latest results: increasing the technological readiness of Laue lenses," SPIE, Astronomical Telescopes and Instrumentation (Jul. 2022). These Proceedings.

[25] Zoglauer, A., Andritschke, R., and Schopper, F., "MEGAlib The Medium Energy Gamma-ray Astronomy Library," *Nar* **50**, 629–632 (Oct. 2006).

[26] Barthelmy, S. D., Barbier, L. M., Cummings, J. R., Fenimore, E. E., Gehrels, N., Hullinger, D., Krimm, H. A., Markwardt, C. B., Palmer, D. M., Parsons, A., Sato, G., Suzuki, M., Takahashi, T., Tashiro, M., and Tueller, J., "The burst alert telescope (BAT) on the SWIFT midex mission," *Space Science Reviews* **120**, 143–164 (oct 2005).

[27] Singh, K. P., "The astrosat observatory," (2022).

[28] Sato, G., Hagino, K., Watanabe, S., Genba, K., Harayama, A., Kanematsu, H., Kataoka, J., Katsuragawa, M., Kawaharada, M., Kobayashi, S., Kokubun, M., Kuroda, Y., Makishima, K., Masukawa, K., Mimura, T., Miyake, K., Murakami, H., Nakano, T., Nakazawa, K., Noda, H., Odaka, H., Onishi, M., Saito, S., Sato, R., Sato, T., Tajima, H., Takahashi, H., Takahashi, T., Takeda, S., and Yuasa, T., "The Si/CdTe semiconductor camera of the ASTRO-H Hard X-ray Imager (HXI)," *Nuclear Instruments and Methods in Physics Research A* **831**, 235–241 (Sept. 2016).

[29] Zhang, F., He, Z., Knoll, G., Wehe, D., and Berry, J., "3d position sensitive cdznte spectrometer performance using third generation vas/tat readout electronics," in [*IEEE Symposium Conference Record Nuclear Science 2004.*], **7**, 4355–4359 (2004).

[30] van Pamelen, M. and Budtz-Jørgensen, C., "Novel electrode geometry to improve performance of cdznte detectors," *Nuclear Instruments and Methods in Physics Research Section A: Accelerators, Spectrometers, Detectors and Associated Equipment* **403**(2), 390–398 (1998).

[31] Abbene, L., Principato, F., Gerardi, G., Buttacavoli, A., Altieri, S., Gong, C., Protti, N., Bettelli, M., Amadè, N. S., Zanettini, S., Zappettini, A., Auricchio, N., Del Sordo, S., and Caroli, E., "New results on high-resolution 3-d czt drift strip detectors," in [*2020 IEEE Nuclear Science Symposium and Medical Imaging Conference (NSS/MIC)*], 1–3 (2020).

[32] Caroli, E., Moita, M., da Silva, R., Del Sordo, S., de Cesare, G., Maia, J., and Pàscoa, M., "Hard x-ray and soft gamma ray polarimetry with cdte/czt spectro-imager," *Galaxies* **6**, 69 (Jul 2018).

[33] Marisaldi, M., Labanti, C., and Soltau, H., "A pulse shape discrimination gamma-ray detector based on a silicon drift chamber coupled to a csi(tl) scintillator: prospects for a 1 kev-1 mev monolithic detector," *IEEE Transactions on Nuclear Science* **51**(4), 1916–1922 (2004).

[34] Nouais, D., Beolè, S., Bondila, M., Bonvicini, V., Cerello, P., Crescio, E., Giubellino, P., Idzik, M., Kolozhvari, A., Kouchpil, S., Torres, E. L., Martinez, M. I., Mazza, G., Piano, S., Piemonte, C., Rashevsky, A., Riccati, L., Rivetti, A., Tosello, F., Trzaska, W. H., Vacchi, A., Wheadon, R., and Alice Collaboration, "The ALICE Silicon Drift Detector system," *Nuclear Instruments and Methods in Physics Research A* **501**, 119–125 (Mar. 2003).